Mesoporous carbon counter electrode materials for dye-sensitized solar cells: the effect of structural mesopore ordering

Ming Chen, Leng-Leng Shao, Xing Qian, Lei Liu, Tie-Zhen Ren, Zhong-Yong Yuan

PII: S1385-8947(14)00852-3
DOI: http://dx.doi.org/10.1016/j.cej.2014.06.103
Reference: CEJ 12347

To appear in: *Chemical Engineering Journal*

Received Date: 26 May 2014
Revised Date: 23 June 2014
Accepted Date: 24 June 2014

Please cite this article as: M. Chen, L-L. Shao, X. Qian, L. Liu, T-Z. Ren, Z-Y. Yuan, Mesoporous carbon counter electrode materials for dye-sensitized solar cells: the effect of structural mesopore ordering, *Chemical Engineering Journal* (2014), doi: http://dx.doi.org/10.1016/j.cej.2014.06.103

Mesoporous carbon counter electrode materials for dye-sensitized solar cells: the effect of structural mesopore ordering

Ming Chen,[a,#] Leng-Leng Shao,[a,#] Xing Qian,[b] Lei Liu,[a] Tie-Zhen Ren,[c] Zhong-Yong Yuan[a,*]

[a] *Key Laboratory of Advanced Energy Materials Chemistry (Ministry of Education), Collaborative Innovation Center of Chemical Science and Engineering (Tianjin), College of Chemistry, Nankai University, Tianjin 300071, China*

[b] *State Key Laboratory of Elemento-Organic Chemistry, College of Chemistry, Nankai University, Tianjin 300071, China*

[c] *School of Chemical Engineering and Technology, Hebei University of Technology, Tianjin 300130, China*

[#] These authors contributed equally.

* Corresponding author. Tel.: +86 22 23509610; fax: +86 22 23502604.

E-mail address: zyyuan@nankai.edu.cn (Z.Y. Yuan).

ABSTRACT. Highly ordered, ordered and disordered mesoporous carbons were prepared by an organic-organic self-assembly method with different molar ratios of formaldehyde to resorcinol (F/R) under the catalysis of citric acid. The mesoporous carbon synthesized with the F/R ratio of 2 possesses highly ordered pore system and large surface area, while the ones with the F/R ratio of 1 and 3 have an ordered and a disordered wormhole-like mesostructure, respectively. These three kinds of mesoporous carbons were utilized as counter electrode (CE) materials for dye-sensitized solar cells (DSSCs) and the effect of structural mesopore ordering on the photovoltaic performance was investigated. The cell assembled with highly ordered mesoporous carbon CE showed an excellent energy conversion efficiency of 6.06%, which is comparable to the one with Pt CE (6.29%), whereas ordered mesoporous carbon and disordered mesoporous carbon CEs based cells exhibited relatively poor photovoltaic performance at the same testing conditions. The enhanced catalytic capability of highly ordered mesoporous carbon CE is intrinsically attributed to the straight channels of long-range highly ordered 2-D hexagonal mesopores, which accelerates the diffusion of redox species and facilitates the charge-transfer process. The synthesized highly ordered mesoporous carbon with outstanding catalytic activity could be an alternative to replace Pt for high-efficiency DSSC CE.

Keywords: Mesoporous carbon; Counter electrode; Dye-sensitized solar cells.

1. INTRODUCTION

Dye-sensitized solar cells (DSSCs) are potential alternatives to conventional silicon solar cells owing to their low cost, simple fabrication process and high energy conversion efficiency[1-4]. Generally, a DSSC consists of a dye-sensitized TiO_2 photoanode, an electrolyte containing a redox couple (I^-/I_3^-) and a counter electrode (CE). As one of the most important components in DSSC, the CE collects electrons from the external circuit and catalyzes the reduction of triiodide ions to iodide ions. Platinum (Pt) is commonly used as the CE material due to its good conductivity for the transport of electrons and excellent electrocatalytic activity for triiodide reduction[5, 6]. However, its high cost and poor stability in corrosive I^-/I_3^- redox system prevent the large-scale commercial application of DSSC in the future[7]. Currently, much effort has been devoted to seeking for the low cost and highly catalytic material to replace the Pt [8]. Carbonaceous materials are quite attractive and expected to be developed as efficient electrocatalysts for DSSCs due to their low cost, high catalytic activity, good electrical conductivity and strong corrosion resistance. To date, various carbon materials, including carbon black [9, 10], activated carbon[11, 12], carbon nanotube [13-15], porous carbon[16, 17], and graphene [18-20], have been investigated as CEs for DSSCs. However, in most cases, the catalytic activities of carbons are still inferior to that of Pt.

To achieve a high power conversion efficiency, the lower intrinsic catalytic activity of carbon compared to that of Pt could be compensated by highly ordered pore structure and the considerably larger active surface area, providing the rapid electrolyte ions diffusion and abundant reduction sites, and hence lowing charge transfer resistance[21]. In consideration of these factors, significant attention should be directed to the ordered mesoporous carbons. Indeed, ordered mesoporous carbons, due to their unique structure, are quite attractive to be used as

novel CE materials for DSSCs [22, 23]. Their highly ordered mesopores and large pore volume are favorable to the transport of electrolyte ions meanwhile the large surface area can offer numerous catalytically active sites for the triiodide reduction.

Generally, the common strategies for the preparation of ordered mesoporous carbon with large surface area and highly ordered pore channels can be classified into soft- and hard-templating methods. Compared to the traditional hard-templating method (nanocasting strategy), the soft-templating route for direct synthesis of ordered mesoporous carbon by organic-organic self-assembly is particularly more attractive due to the avoidance of many drawbacks such as multistep synthesis, time-consuming, and high cost [24-26]. This method involves a combination of polymeric precursors acting as the carbon source, a tri-block copolymer playing the role of a soft template, and acid or base functioning as the polymerization catalyst[24, 27, 28]. Phenolic resin is the most frequently used polymeric precursor for the synthesis of ordered mesoporous carbon. Specially, hydrochloric acid (HCl) and NaOH are often served as the catalysts for the preparation of resorcinol (R)-formaldehyde (F) resin [27, 29]. However, the use of NaOH and HCl results in the corrosion of the equipment and the pollution of halogenide ions. Some alternative catalysts such as citric acid [30] and amino acid [31, 32] were successfully developed to catalyze the polymerization of RF resin, which is more flexible and convenient in preparing ordered mesoporous carbon than other soft-template methods with HCl or NaOH as catalyst. In these green synthesis systems, the ordered mesostructures were obtained by controlling the amount of catalysts. Apart from catalysts, it has been well demonstrated that the F/R molar ratio is another crucial parameter in preparing ordered mesoporous carbon under the catalysis of HCl [28]. However, the influence of F/R molar ratio on the ordered mesostructure under the catalysis of citric acid or amino acid was not reported yet [30-32]. The exploration of appropriate F/R

molar ratio to obtain high-purity and well-structured mesoporous carbons under the synthesis system with new catalysts should be required for the practical application. Moreover, with regard to the specific application of mesoporous carbon as CE for the DSSC, the structural mesopore ordering may be one of crucial factors affecting the electrocatalytic activity. The construction of ordered mesopore channels in the high-surface-area mesoporous carbon may result in the enhanced properties compared to the disordered mesopore channels due to the higher-rate ions transport capacity arising from ordered mesopore channels. So far, no reports have been reported the correlation between the mesopore ordering and the electrocatalytic activity of mesoporous carbon CEs.

Herein, we utilized citric acid as catalyst to directly synthesize mesoporous carbons by organic-organic self-assembly with resorcinol and formaldehyde as the polymer monomers and F127 as the mesopore template. By simply tuning the F/R molar ratio, three kinds of mesoporous carbons with different levels of ordered mesostructure were obtained. When used as CEs for DSSCs, three kinds of mesoporous carbons displayed different behaviors toward the triiodide reduction, and hence resulting in the different photovoltaic performance of DSSCs. Specifically, the relationship between the mesopore ordering and the photovoltaic performance of DSSCs based on mesoporous carbon CEs was discussed.

2. EXPERIMENTAL SECTION

2.1 Preparation of mesoporous carbons. Mesoporous carbons were synthesized by a low-temperature autoclaving method. In the synthesis, 1.65 g of resorcinol and 2.5 g of F127 were dissolved in a mixture of 20 ml of water and 20 ml of ethanol, stirring for 30 min until the solution turned into colorless, followed by the addition of 2.9 g of citric acid to act as a catalyst.

After 1 h of stirring, 2.5 g of 37% formaldehyde solution was added dropwise under tempestuously stirring. The reaction mixture was further vigorously stirred for another 1 h, and a homogeneous colorless solution was obtained, which was then transferred to a Teflon-lined autoclave and heated at 60 ºC for 3 days. The resulting polymeric monolith was washed with ethanol and water, dried in an oven at 60 ºC for 12 h. Carbonization was carried out in a tubular furnace under an inert atmosphere (N_2 flow) with a heating rate of 1 ºC/min, and then keeping the temperature at 800 ºC for 3 h. The final product was denoted as MC-2 (considering the precursor F/R ratio of 2:1). When adjusting the F/R ratio to 3:1 during the synthesis, the resultant carbon was denoted as MC-3. When the synthesis was performed with the F/R ratio of 1:1, the Teflon-lined autoclave was maintained at 60 ºC for 3 days and subsequently at 80 ºC for 2 days, and the obtained carbon was labeled as MC-1.

2.2 Preparation of carbon and Pt CEs. The mesoporous carbon CEs were prepared with a simple doctor-blade method as follows: A mixture of 130 mg of mesoporous carbon MC-*x* (*x* represents the F/R ratio) and 15 mg of PEG-2000 was ultrasonically dispersed in 3 ml of deionized water and then continuously stirred for 4 h to form a mixed suspension. Meanwhile, 20 mg of TiO_2 (P25, Degussa, Germany) in 2 ml of water was also ultrasonically dispersed for 30 min and stirred to form a white TiO_2 colloid. Then the TiO_2 colloid was mixed with the prepared carbon suspension and stirred continually for 3 h to form the final paste. The paste was scraped onto a FTO (fluorine-doped tin oxide) conductive glass (14 Ω/□, Nippon Sheet Glass) by the doctor-blade method to prepare a film and then dried at 80 ºC overnight. The mesoporous carbon MC-*x* CEs were finally obtained. For the sake of comparison, carbon black (40 nm in particle size, Timcal, Taiyuan, China) CEs were prepared by the same procedure. Pt CEs were fabricated

by conventional thermal decomposition of 30 mM $H_2PtCl_6 \cdot 6H_2O$ solution spin-coated on the surface of FTO at 400 ºC for 30 min.

2.3 Preparation of DSSCs. The dye-sensitized TiO_2 photoanode was prepared as follows: FTO conductive glass was firstly treated with 50 mM $TiCl_4$ aqueous solution at 70 ºC for 30 min. A *ca*. 5 μm thick layer of 20 nm-sized TiO_2 particles (Degussa, Germany) was printed on FTO by doctor-blading technique and dried at 125 ºC for 15 min. The obtained layer was further coated with a *ca*. 3 μm thick scattering layer of 200 nm-sized TiO_2 particles and calcined at 450 ºC for 30 min, followed by cooling to room temperature. The calcined electrode was treated with 50 mM $TiCl_4$ aqueous solution at 70 ºC for 30 min, washed with distilled water, recalcined at 450 ºC for 30 min. After cooling to room temperature, the TiO_2 film was immersed in a 0.3 mM N719 dye (Solaronix SA, Switzerland) ethanol solution overnight. Finally, it was cleaned with ethanol and dried to obtain a dye-sensitized TiO_2 film. The DSSC was assembled with a dye-sensitized TiO_2 photoanode, a counter electrode and an electrolyte containing 0.05 M I_2, 0.5 M LiI, 0.3 M 1,2-dimethyl-3-propylimidazoliumiodide (DMPII), and 0.5 M 4-tert-butyl pyridine with acetonitrile as the solvent. The aperture of the scotch tapes coated on FTO was used as the electrolyte storage spacer. The two electrodes were clipped together and the active area was 0.20 cm^2.

2.4 Characterization. Powder X-ray diffraction (XRD) patterns were recorded on a Bruker D8 Focus diffractometer, with Cu K_α radiation (λ = 1.5406 Å) operated at 40 kV and 40 mA. Transmission electron microscopy (TEM) measurements were performed on a JEOL JEM 2010 microscope at 200 kV. All samples subjected to TEM measurements were ultrasonically dispersed in ethanol and drop-casted onto copper grids covered with carbon film. Nitrogen adsorption-desorption isotherms were measured on a Quantachrome NOVA 2000e sorption

analyzer at 77 K. The specific surface area (S_{BET}) was calculated by the Brunauer–Emmett–Teller (BET) method, the pore size distributions were derived from the adsorption branches of isotherms using BJH method, and the total pore volumes (V_{total}) were estimated from the adsorbed amount at a relative pressure P/P_0 of 0.980. Raman spectroscopy was performed on a Renishaw-1000 Raman spectrometer (Renishaw, UK).

2.5 Electrochemical measurement. The photovoltaic characteristics of sealed DSSCs were measured under simulated AM 1.5 illumination (I = 100 mW cm^{-2}) with a solar simulator (CHF-XM500, China). Cyclic voltammetry (CV) measurements were conducted in a three-electrode system in acetonitrile solution at a scan rate of 50 mV s^{-1}, using a Zennium electrochemical workstation (Zahner, Germany). The prepared mesoporous carbon, carbon black and Pt/FTO electrodes were used as working electrodes, Pt/FTO as auxiliary electrode, and Ag/Ag^+ electrode as reference electrode. The electrolyte contained 0.1 M $LiClO_4$, 10 mM LiI, and 1 mM I_2 in acetonitrile. Electrochemical impedance spectroscopy (EIS) and Tafel polarization measurements were carried out on a Zahner Zennium electrochemical workstation in a symmetrical dummy cell consisted of two identical CEs. The geometric area of the symmetrical dummy cell was 0.25 cm^2. EIS spectra were obtained with an AC modulation signal of 10 mV and bias DC voltage of -0.60 V over the frequency range of 100 kHz to 100 mHz in dark condition. Tafel polarization measurements were performed at a scan rate of 10 mV s^{-1}.

3. RESULTS AND DISCUSSION

3.1 Synthesis and material characteristics. As RF resol is well known as the mesoporous carbon precursor, the well-organized mesostructured resin polymers can be of great guarantee for the successful preparation of ordered mesoporous carbon. The formation of well-structured resin

polymers is remarkably dependent on self-assembly between the template F127 and RF resin, in which a large number of hydroxyl groups in resol formed from resorcinol provide the great driving force for the interaction with the PEO blocks of F127 through hydrogen bonding[27]. The macroscopic phase separation of the polymer-rich phase from the ethanol/water solvent is the key step in the generation of carbon precursor/F127 composite accompanied by the polymerization between the resorcinol and formaldehyde in an acidic system [33-35]. The molar ratio of formaldehyde to resorcinol (F/R) plays an important role in regulating the phase separation process under the fixed amount of catalyst and F127. To investigate the influence of F/R molar ratio on the structure of mesoporous carbon, samples were synthesized by varying the F/R molar ratio from 1 to 3 and fixing the molar ratio of formaldehyde to citric acid at 6:1. It is noteworthy that phase separation phenomenon occurred when the molar ratio of F/R is 2 or 3, while no products were achieved when the F/R molar ratio is 1 under the reaction temperature of 60 ℃. Thus for the synthesis system with the F/R molar ratio equal to 1, the reaction temperature was subsequently increased to 80 ℃ in order to accelerate the phase separation and obtain the polymer-rich products. After carbonization at 800 ℃, mesoporous carbons were obtained with variable pore structure ordering based on the F/R molar ratio.

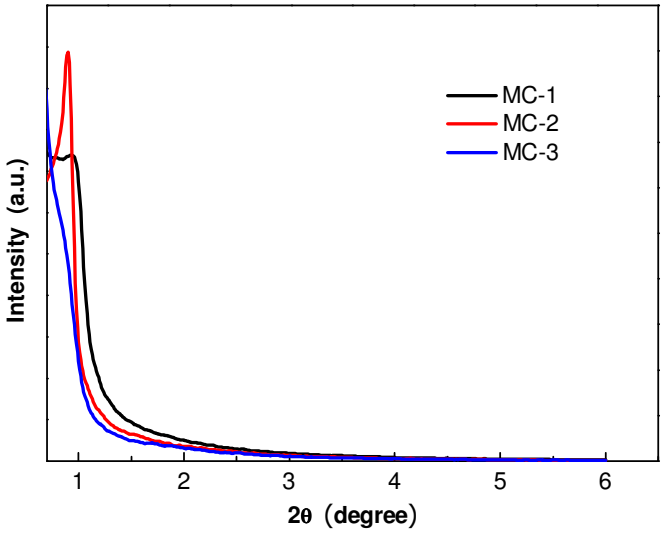

Figure 1. Low-angle XRD patterns of the synthesized mesoporous carbons.

Figure 1 shows the low-angle XRD patterns of the obtained mesoporous carbon materials by tuning the F/R molar ratio. MC-1 and MC-2 display the characteristic low-angle peaks of mesoporous materials at 0.89º and 0.93º (2θ), respectively, which can be indexed as (100) reflection of the 2-D hexagonal *p6mm* mesostructure [36]. However, the diffraction peak of MC-2 is obviously sharper than that of MC-1, indicating a higher structural mesopore ordering. In the case of MC-3, the low-angle XRD pattern presents a slope line instead of the characteristic peaks, demonstrating a poor long-range mesopore ordering. This is further confirmed by TEM images (Figure 2). As shown in Figure 2, the orderly hexagonal arrangement of mesoporous structure for MC-1 and MC-2 can be clearly observed. Particularly, MC-2 shows a well ordered long-range hexagonal arrangement along the [001] and [110] directions, revealing its highly ordered mesostructure. However, MC-1 shows the inferior periodic ordering compared to that of the MC-2, and MC-3 exhibits worm-like pores with the worst mesopore ordering.

The pore structure of the prepared carbons was evaluated by nitrogen sorption analysis. Figure 3 shows N_2 adsorption-desorption isotherms of the prepared carbons and the corresponding pore

size distributions. The textural properties are summarized in Table 1. The isotherms of MC-1, MC-2 and MC-3 display the similar and typical type-IV curves with obvious hysteresis loops at relative pressure of 0.45-0.80, indicating the well-developed mesoporous structures of materials with cylindrical channels [37]. The pore size distributions (Figure 3b), calculated from the adsorption branches using the BJH method, of MC-2, MC-1 and MC-3 present narrow peak in the range of 2.4-6.2, 2.4-5.5 and 2.4-6.2 nm, respectively. The MC-2, MC-1, and MC-3 possess a large BET surface area of 667, 595 and 616 m^2g^{-1}, and a total pore volume of 0.63, 0.49 and 0.56 cm^3g^{-1}, respectively. However, the commercial carbon black displays type III isotherms, suggesting its poor porosity. The BET surface area of carbon black is 136 m^2g^{-1}, which is quite lower than that of the prepared mesoporous carbons.

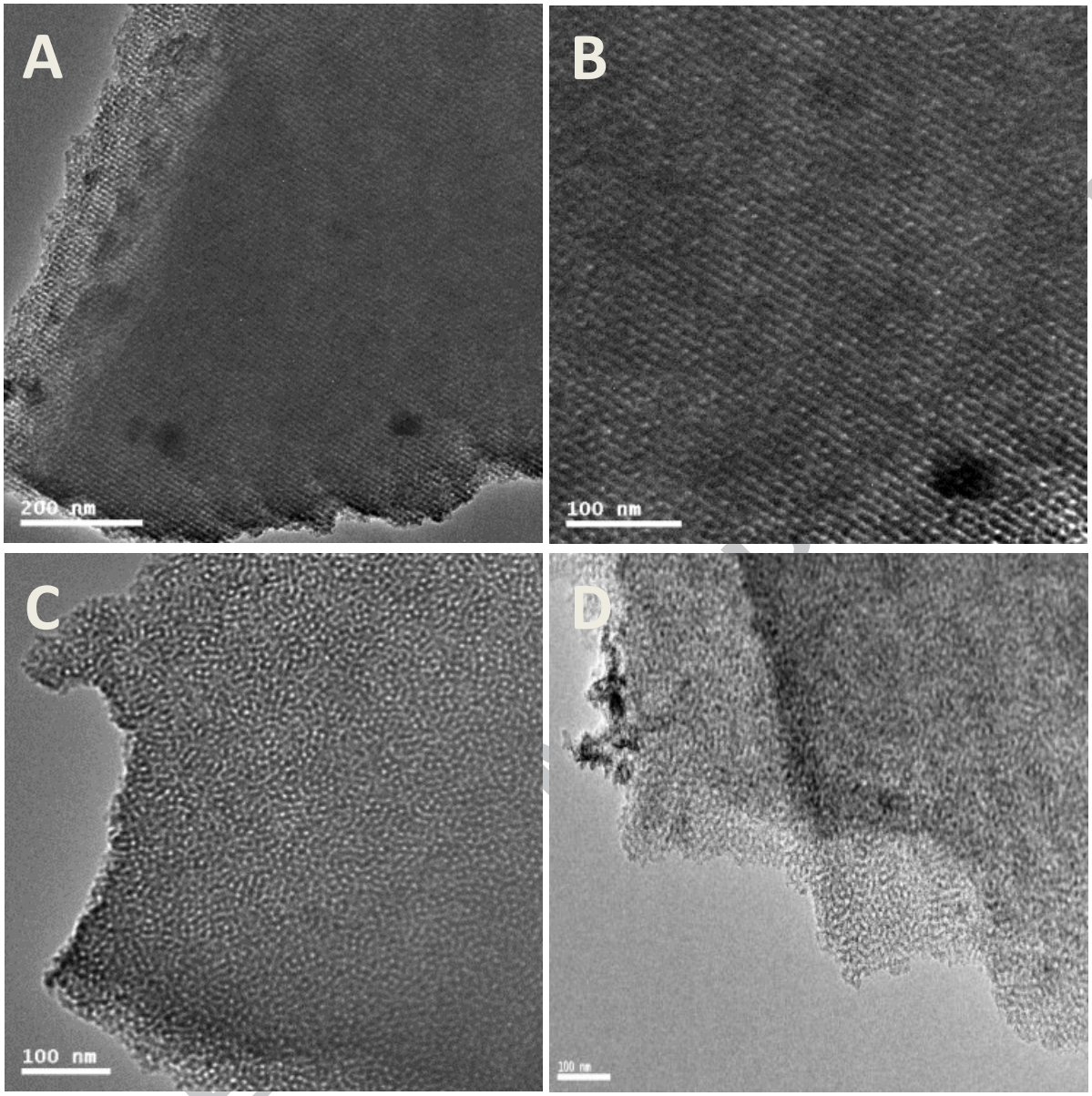

Figure 2. TEM images of the synthesized mesoporous carbons: MC-2(A, B), MC-1 (C) and MC-3 (D).

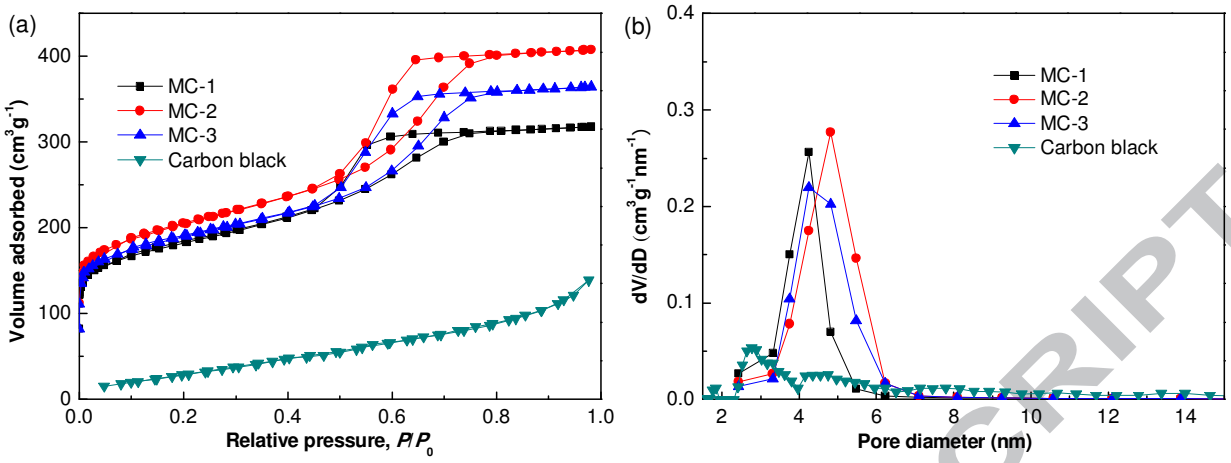

Figure 3. (a) N_2 adsorption-desorption isotherms of the synthesized mesoporous carbons and (b) the corresponding BJH pore size distribution curves.

Table 1. Structural and Textural Properties of the Synthesized Mesoporous Carbons.

Sample	F/R ratio	S_{BET} [a] (m^2g^{-1})	S_{micro} [b] (m^2g^{-1})	V_{total} (cm^3g^{-1})	V_{micro} [b] (cm^3g^{-1})	D_{BJH} [c] (nm)	d_{100} [d] (nm)	a_0 [d] (nm)	t [e] (nm)
MC-1	1	595	377	0.49	0.12	4.3	9.5	11.0	6.7
MC-2	2	667	395	0.63	0.14	4.8	9.9	11.4	6.6
MC-3	3	616	341	0.56	0.14	4.3	-	-	-

[a] The BET surface area S_{BET} calculated using adsorption data in a relative pressure range P/P_0 = 0.05–0.24. [b] The micropore surface area S_{micro} and the micropore volume V_{micro} obtained by the *t*-plot method. [c] The pore size D_{BJH} obtained from the maxima of the pore size distribution curve calculated by the BJH method. [d] The d-spacing of the (1 0 0) diffraction $d_{(100)}$, and unit cell parameter a_0 calculated from the XRD patterns by $a_0 = 2d_{(100)}/\sqrt{3}$. [e] Pore wall thickness calculated as thickness $t = a_0 - D_{BJH}$.

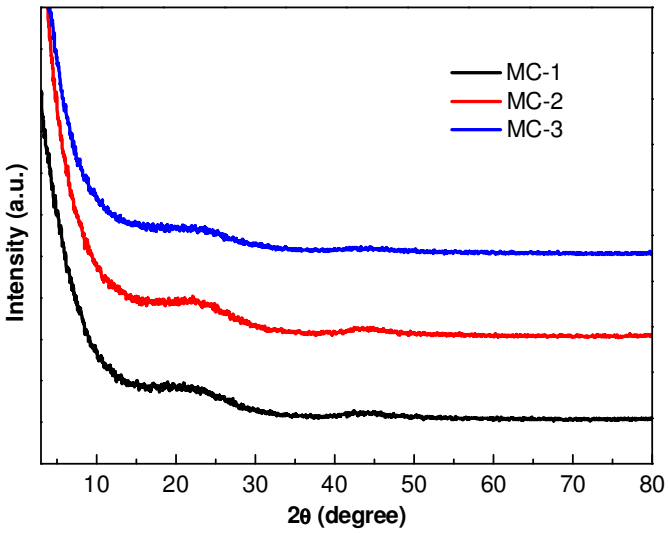

Figure 4. Wide-angle XRD patterns of the synthesized mesoporous carbons.

The wide-angle XRD patterns (Figure 4) show broad diffraction peaks for the prepared mesoporous carbons at 2θ of *ca.* 22.9º which are assigned to the amorphous carbons. The very weak diffraction peaks in XRD patterns at 2θ of *ca.* 26º and 43.8º correspond to the (0 0 2) and (1 0 1) diffractions of typical graphitic carbons [38], respectively, suggesting the partial graphitization in the amorphous frameworks of the prepared mesoporous carbons [39]. The structure of carbon material was also studied by the Raman spectroscopy (Figure 5). As shown in Figure 5, the MC-2 shows two strong and broad bands at 1316 and 1586 cm^{-1} that ascribed to the D and G bands of the disordered and graphitic carbons, respectively. The relative intensity ratio of G-band to D-band (I_G/I_D) depends on the type of graphitic materials and is proposed as the indicator of graphitization degree of these carbon materials [40, 41]. The I_G/I_D for MC-2 is 0.48, indicating that the highly ordered mesoporous carbon is composed of plentiful amorphous carbon and partially graphitic carbon.

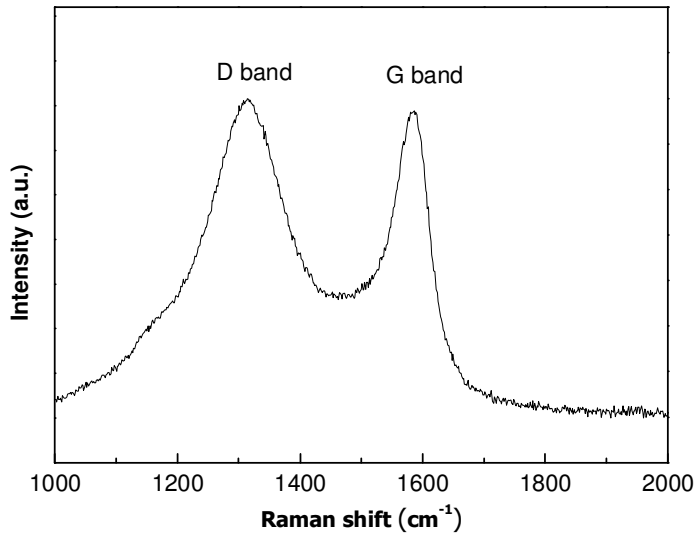

Figure 5. The Raman spectrum of MC-2 sample.

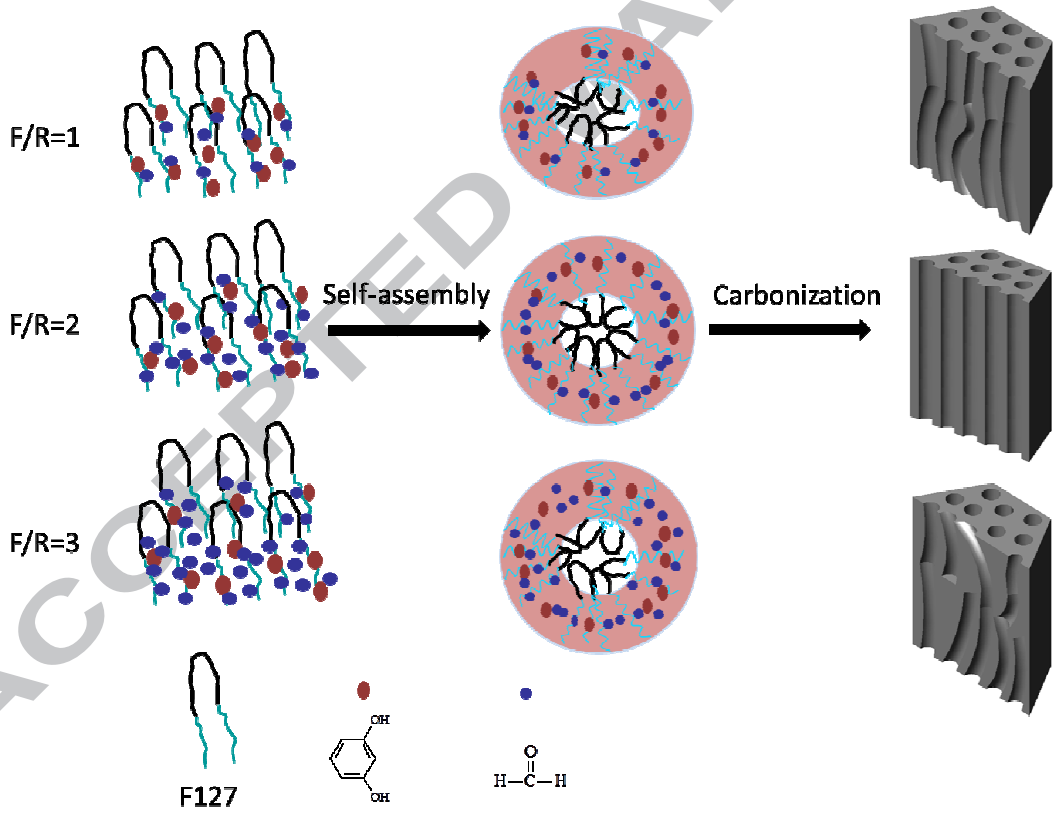

Figure 6. Schematic illustration of the synthesis of mesoporous carbons from the precursors with different F/R molar ratios.

As observed from various textural characteristics of three kinds of mesoporous carbons, the mesopore ordering is of dominating difference. It is deduced that the mesopore ordering is closely associated with the F/R molar ratio (Figure 6). When the F/R molar ratio is fixed to 1, no macroscopic phase separation occurred under the catalysis of critic acid, which is different from the previous report that well-defined mesoporous carbon precursor was obtained with the HCl as catalyst[28]. To the best of our knowledge, the concentration of acid and the reactivity of resorcinol are two key factors in determining the polymerization rate of phenolic resins [27]. In the presence of an acid catalyst, resorcinol reacts with formaldehyde slowly at low temperature to produce low cross-linked polymers. Upon the hydrothermal treatment, the strong and collective interactions among the reacting species quickly result in the high condensation degree of RF resol with highly cross-linked polymers, and finally lead to the generation of phase separation. In this work, although the excess amount of R would enhance the interaction between the RF polymer and the F127 via hydrogen bond, the relatively lower concentration of critic acid compared to that of HCl remarkably decreased the polymerization rate, thus resulting in no appearance of sedimentation. To solve this problem, the reaction temperature was subsequently adjusted to 80 ºC. The great driving force for the self-assembly process at 80 ºC led to the formation of MC-1. However, the higher reaction temperature reduced hydrogen bond interaction between the RF polymer and the F127, and motivated the polymerization of the resorcinol/formaldehyde oligomers to high-molecular-weight resol polymer particles instead of assembling with the PEO segments, which led to a lower mesopore ordering compared to the MC-2 [30]. The attractive structural characteristics of MC-2 with highly ordered mesopore ordering benefit from the appropriate F/R ratio at suitable crystallization temperature. However, when the F/R molar ratio is up to 3, the disordered mesopores were observed in MC-3. As

demonstrated in our previous work[28], excessive amount of F may act as a curing agent, but it can also induce the aggregation of the oligomer, and affect the self-assembly of the precursor and template by consuming the hydroxyl groups of the resol. The reduction of the hydroxyl groups of the resol weakened the interaction between resol and F127, which initiated the collapse of mesopore structure to disordered worm-like mesopores. It can be concluded that the precursor aggregates should be small enough by adjusting the F/R molar ratio to enable assembly around F127 micelles for the formation of the well-defined mesostructured RF/F127 composite. Indeed, the molar ratio of F/R is a crucial factor in determining the self-assembly process and the structure of the mesoporous carbons.

3.2 Electrocatalytic activity in DSSCs. CE is one of the important parts in DSSC and its high performance on catalyzing the reduction of triiodide is of prime concern. The prepared mesoporous carbons not only supply abundant active sites for catalyzing I_3^- to I^- from numerous defect sites in these amorphous carbons, but provide efficient ions transport from their wider mesopores than the size of electrolyte ions [23]. What's more, mesopores act mostly as an electrolyte supply to micropores, offering a larger ion-accessible surface area. On the other hand, the ordering of mesopores can also impact the electrocatalytic activity of CE, especially for fast triiodide reduction reaction when any impediment to the transport of electrolyte ions becomes critical. To clarify this issue, the comparison between similar mesoporous carbons, mainly differing in mesopore ordering, can be of great help. Thus, highly ordered (MC-2), ordered (MC-1) and disordered (MC-3) mesoporous carbons were applied as CEs to specifically study the effect of mesopore ordering on the electrocatalytic activity of carbon CEs and photoelectrical performance of DSSCs based on carbon CEs.

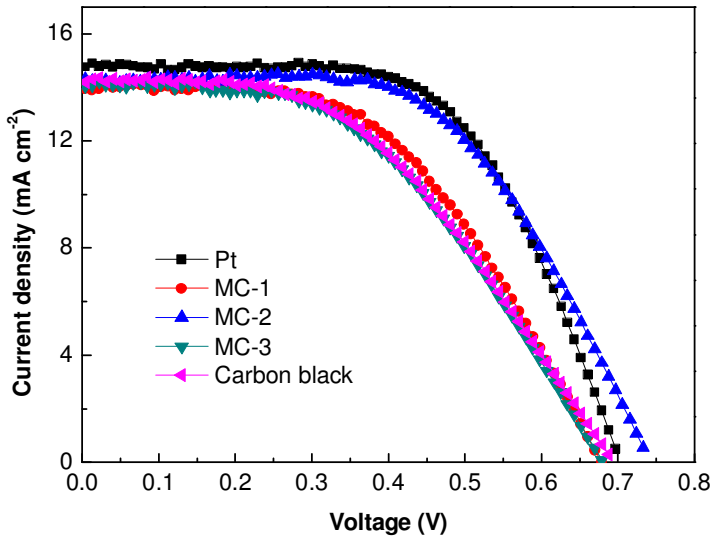

Figure 7. Photocurrent-voltage characteristics of the cells using mesoporous carbon, carbon black and Pt CEs.

J-V characteristic curves of DSSCs using mesoporous carbon, carbon black and Pt CEs are presented in Figure 7, and the corresponding photovoltaic and electrochemical performance parameters of the cells are summarized in Table 2. The devices with MC-2, MC-1 and MC-3 as CEs displayed an open-circuit voltage (V_{oc}) of 0.733, 0.679 and 0.679 V, short-circuit current density (J_{sc}) of 14.32, 13.94 and 14.04 mA cm^{-2}, fill factor (*FF*) of 0.58, 0.52 and 0.48, and conversion efficiency (η) of 6.06%, 4.88% and 4.58%, respectively. Obviously, the η and *FF* of DSSCs assembled with mesoporous carbon CEs shift to lower values in the order of MC-2, MC-1, and MC-3 CE, indicating a reduced catalytic activity toward the triiodide reduction, in accordance with the ordering degree of the MC-*x* mesostructure. The reduction of catalytic activity may be attributed to the slower diffusion rate of electrolyte ions along with the decrease of structural mesopore ordering. Therefore, the structural mesopore ordering may become a decisive factor impacting the rate of reduction reaction in following ways (Figure 8): first, highly ordered two-dimensional mesopore channels for the MC-2 would shorten the electrolyte ions

transfer distance compared to the tortuous channels of MC-1 and MC-3. So it would take less time for ions to arrive at the active sites distributed on the porous surface when they were transported into the internal surface of the MC-2 particles. As electrolyte ions moved in the two-dimensional ordered mesoporous channels along one direction in mesoporous carbon particles, if the mesopore channels are regularly arranged, with high ordering and fewer flaws such as pore fracturation, dislocation, tortuousness and even the impurities, the electrolyte ions would pass straightly through one side of the particle to the end and complete the rapid triiodide reduction on the defect sites of carbon with less electrons recombination. Second, highly ordered mesopores supply fast ions diffusion channels to reach the micropores which enlarge the utilization of the surface areas belonged to the micropores. As the ions could be transported timely to the catalytic active sites distributed on the microporous surface through mesoporous channels, the catalytic kinetics for the reduction of triiodide could be extremely accelerated. Theoretically, faster ions diffusion in combination of higher catalytic kinetics would grant higher catalytic activity of MC-2 CE.

Table 2. Photovoltaic and Electrochemical Parameters of DSSCs with Different Counter Electrodes

Counter electrode	V_{oc} (V)	J_{sc} (mA cm^{-2})	*FF*	□ (%)	R_s (□)	R_{ct} (□)
Pt	0.697	14.77	0.61	6.29	36.2	17.2
MC-1	0.679	13.94	0.52	4.88	31.1	13.1
MC-2	0.733	14.32	0.58	6.06	29.3	10.5
MC-3	0.679	14.04	0.48	4.58	34.6	15.7
Carbon black	0.688	14.19	0.47	4.61	31.7	33.5

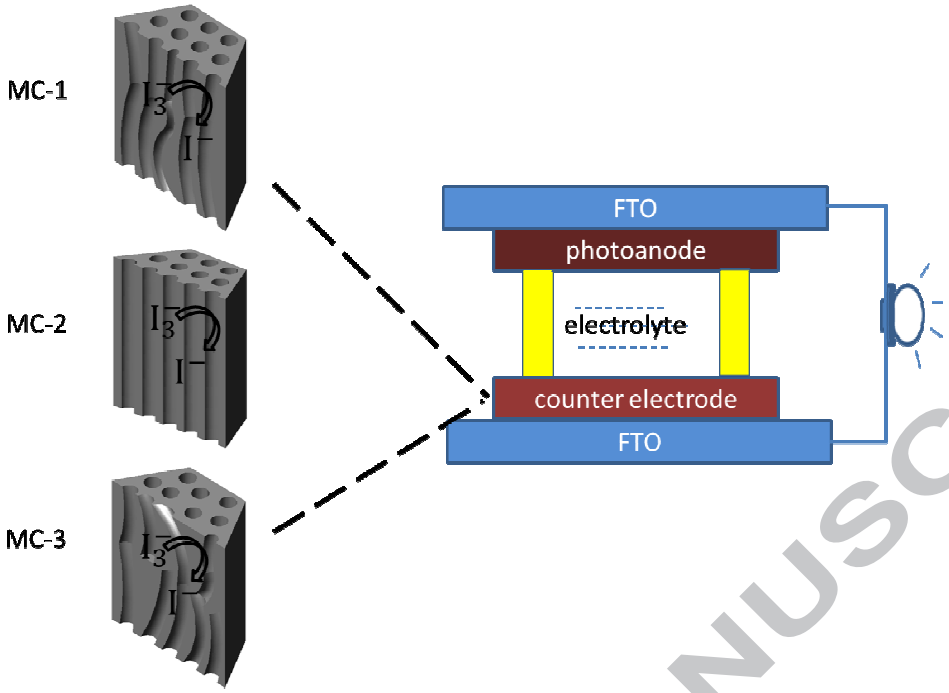

Figure 8. Illustration of the influence of mesopore ordering on the electrocatalytic activity of mesoporous carbon CEs in DSSCs.

It is also worth mentioning that the improvement on the V_{oc} can further confirm the facile reduction reaction on the MC-2 CE compared to MC-1 and MC-3 CEs. Generally, V_{oc} is the difference between the electronic Fermi level (E_f) of the TiO_2 semiconductor and the redox potential of the I^-/I_3^- (φ_{I^-/I_3^-}) on the CE, which can be calculated by eq. 1 [42].

$$V_{oc} = \left| E_f - \varphi_{I^-/I_3^-} \right| \qquad (1)$$

Assuming that I^-/I_3^- electrolyte and TiO_2 semiconductor remain unchanged, V_{oc} depends directly on the electrochemical properties of the CE. The positive shift of redox potential on the CE, and extra charge at the double-layer capacitor which arises from interface of the large-surface-area MC electrode and electrolyte are two possible explanations for the improved V_{oc} [23, 43]. The V_{oc} value of the DSSC with MC-2 CE is higher than those of the cells with MC-1

and MC-3 CEs, indicating a superior catalytic activity of MC-2 for the I^-/I_3^- redox couple among the mesoporous carbons. The superior catalytic activity is intrinsically associated with the unique structure of MC-2. Highly ordered mesopore channels provide the quick diffusion of redox species, thus leading to fast reduction of I_3^- on the abundant ion-accessible active sites of carbon material. The efficiency of the DSSC with MC-2 CE is almost equal to that of the cell based on the Pt CE (6.29%) at the same testing conditions. However, the DSSC based on MC-3 CE achieved the lowest η due to inefficient ions diffusion in the disordered and tortuous mesoporous channels. For the DSSC assembled with conventional carbon black CE, low surface area and small-sized pores resulted in lower η than that of MC-2 and MC-1 CEs, but slightly higher η than that of MC-3 CE.

To investigate the catalytic activity of various CEs, electrochemical impedance spectra (EIS) were measured using symmetrical dummy cells assembled with two identical CEs [44, 45]. In the obtained Nyquist plots of MC CEs in Figure 9, the intercept on the real axis can be generally attributed to the series resistance (R_s) and the semicircle in high frequency region corresponds to the charge-transfer resistance (R_{ct}) in the electrode/redox electrolyte interface for I^-/I_3^- redox reaction and the corresponding capacitance (CPE). The low frequency region is mainly assigned to the Nernst diffusion resistance (Z_w) of I^-/I_3^- redox species in the electrolyte [46]. While different from those of MC CEs, the EIS of carbon black showed three semicircles at high, middle and low frequency from left to right, which are correspondingly ascribed to the charge transport resistance(R_{trns}) in parallel with the capacitance (C_{trap}), the charge transfer resistance (R_{ct}) in parallel with the corresponding double layer capacitance(CPE), and the Nernst diffusion impedance (Z_w) in the electrolyte [9, 10]. The R_{ct} is a key parameter which is closely related to the intrinsic electrocatalytic activity of CE material for the reduction of

triiodide[12, 47]. It is obtained by estimating the diameter of the high-frequency semicircle and summarized in Table 2. It is worth noting that the R_{ct} values of MC-2, MC-1, MC-3, Pt and carbon black are 10.5, 13.1, 15.7, 17.2, and 33.5 Ω, respectively, suggesting that MC-2 has better electrocatalytic activity than those of MC-1 and MC-3 for the reduction of triiodide. Moreover, the mesoporous carbons possess lower charge transfer resistance than those of the Pt and carbon black CEs. This could be attributed to the improved ions transportation capacity in the ordered mesoporous channels especially in the highly ordered ones. In addition, the surface areas of the mesoporous carbons (595 – 667 m^2g^{-1}) are obviously larger than that of carbon black (136 m^2g^{-1}), which provide abundant electrocatalytic active sites for I_3^- reduction, resulting in the lower R_{ct} of mesoporous carbon CEs [48]. However, the Warburg impedance of the mesoporous carbon CEs in the low-frequency region (slope of the warburg line) is slightly larger than that of Pt CE, leading to the unfavorable consequence for electrocatalytic activity. It probably resulted from the thick mesoporous carbon layers which provide longer ions pathway compared with the thin Pt film [49]. In addition, the R_s values of MC-2, MC-1 and MC-3 CEs are slightly lower than 36.2 Ω of Pt, suggesting that the mesoporous carbons have been kept good adhesion to the FTO [50]. Photovoltaic performance of DSSCs with mesoporous carbon CEs may be influenced by the two positive factors of good adhesion and low R_{ct}, which lead to high conversion efficiencies.

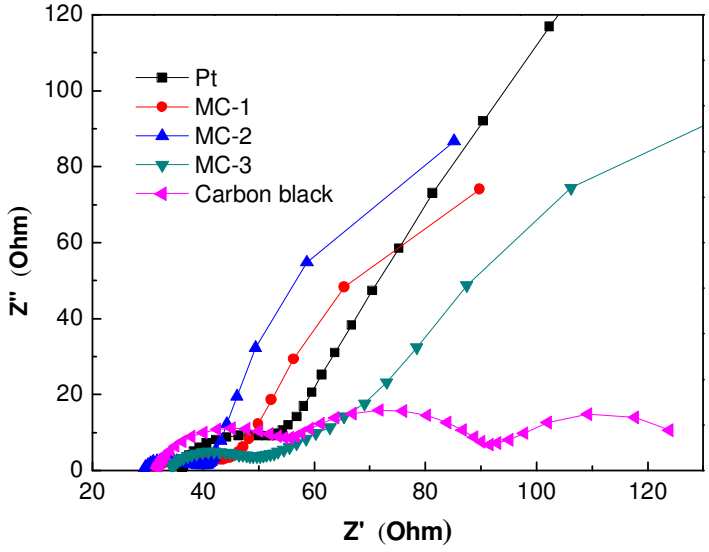

Figure 9. Nyquist plots of the symmetrical cells with two identical mesoporous carbon, Pt, and carbon black CEs.

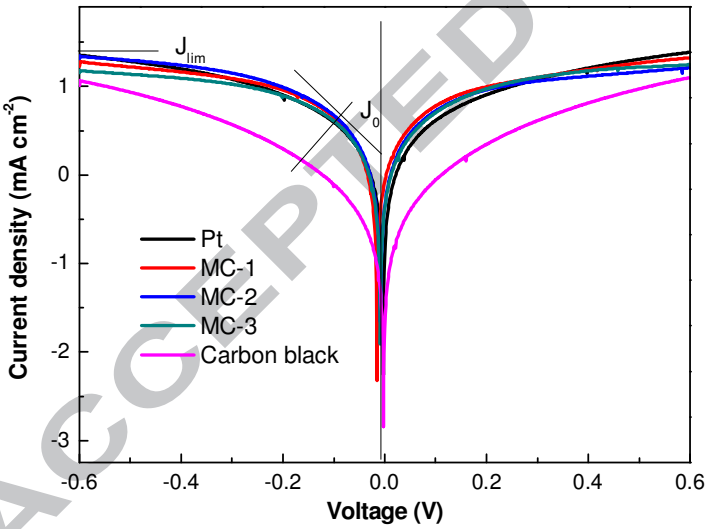

Figure 10. Tafel polarization curves of symmetrical cells based on the mesoporous carbon, Pt, and carbon black CEs.

To further confirm the catalytic activities of MC-2, MC-1 and MC-3 CEs, Tafel polarization measurements were also carried out with the cells used in the EIS test [51]. As shown in Figure 10, a larger slope for the MC-2 CE is observed in comparison with that of MC-1, MC-3 and carbon black CEs, indicating a higher exchange current density (J_0) [46, 52]. It is found that J_0 of mesoporous carbons decreases slightly with the decline of mesopore ordering, but much higher than that of carbon black, which also demonstrates the effect of mesoporous channels on the reduction reaction. Furthermore, the large J_0 for the MC-2 CE is even higher to that of Pt, implying that it could effectively catalyze the reduction of triiodide to iodide. Besides, the J_0 can be expressed as eq. 2 [53],

$$J_0 = \frac{RT}{nFR_{ct}} \tag{2}$$

where R_{ct} is extracted from the electrochemical impendence spectra, T is the absolute temperature, R is the gas constant, n is the total number of individuals, and F is the Faraday constant. The large J_0 means that there is a low charge-transfer resistance (R_{ct}) at the electrolyte-electrode interface, which is consistent with the EIS measurements. In addition, J_{lim} is determined by the diffusion of the redox couple in the electrolyte, as presented in eq. 3 [52],

$$D = \frac{l}{2nFC} J_{lim} \tag{3}$$

where D is the diffusion coefficient of the triiodide, l is the spacer thickness, n is the number of electrons involved in the reduction of triiodide at the electrode, F is the Faraday constant, and C is the triiodide concentration. A higher limiting current density (J_{lim}) for the MC-2 is also shown in Figure 10 compared to MC-1 and MC-3, indicating a faster diffusion velocity for the redox couple owing to its highly ordered mesopore channels [44]. Indeed, highly ordered mesopore channels reduced the penetration pressure and shortened the transportation distance which

increased the ions transfer efficiency. Whereas, in comparison with the mesoporous carbons, poor porosity of the carbon black makes it difficult for electrolyte ions diffusion in the interior of the material, and consequently a much smaller J_{lim} was observed, verifying the slow diffusion velocity for the redox couple.

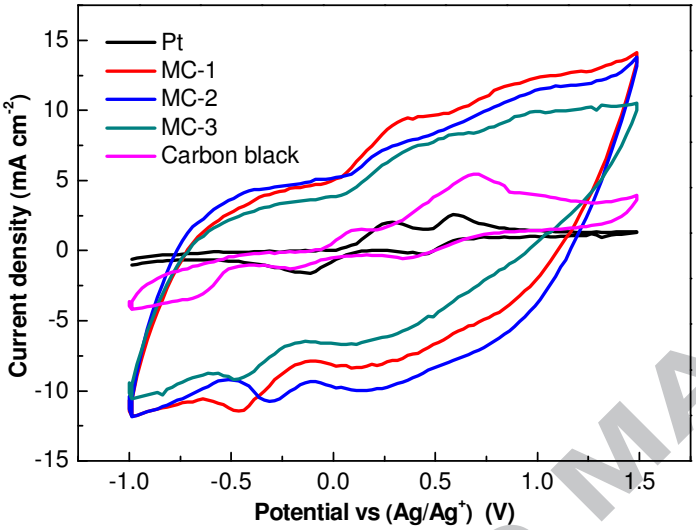

Figure 11. Cyclic voltammetry curves of mesoporous carbon, Pt, and carbon black CEs at a scan rate of 50 mV s^{-1} in 10 mM LiI, 1 mM I_2 and 0.1 M $LiClO_4$ acetonitrile solution. Reference electrode: Ag/Ag^+ in acetonitrile. Auxiliary electrode: Pt/FTO.

To further examine the electrocatalytic activity for the reduction of I_3^- on various CEs, CV measurements were carried out in a three-electrode system at a scan rate of 50 mV s^{-1} [46]. As shown in Figure 11，two pairs of redox peaks are observed for the Pt and carbon black CEs. The left pair in the low potential range is assigned to the redox reaction shown in eq. 4 and the right pair in the high potential range is assigned to the redox reaction shown in eq. 5 [11, 54].

$$I_3^- + 2e \leftrightarrow 3I^- \quad (4)$$

$$3I_2 + 2e \leftrightarrow 2I_3^- \quad (5)$$

The redox reaction shown in eq. 4 is the rate-determining step to transfer electrons from the counter electrode to the electrolyte for the reduction of triiodide ions at -0.15 V [55]. However, the reduction peaks of mesoporous carbons are more negative than those of the Pt (*ca.* -0.15 V) and carbon black (*ca.* -0.19 V), suggesting a slow redox reaction at the MC-*x* CEs. Nevertheless, the mesoporous carbon CEs exhibit much higher current density than the Pt and carbon black CEs, due to the numerous reduction reactions of triiodide to iodide on the large ion-accessible surface area arising from advantageous structural characteristics of large surface area and mesoporous structure, implying higher catalytic activity [23, 56]. Importantly, in the case of similar oxidation peak potentials of MC-*x* CEs, the reduction peak potential for I^-/I_3^- redox reaction at MC-2 CE (-0.313 V) is more positive compared with those of MC-1 and MC-3 CEs, indicating a more reversible redox reaction and higher reduction reaction rate. Additionally, it is well known that the redox reaction is controlled by ions diffusion which may be related to the transport of triiodide species on the CE surface [57]. It is expected that the improved ions diffusion rates in the highly ordered mesopore channels are beneficial for the I_3^- to achieve the reactive sites motivated by the concentration grades and to be adsorbed by the reactive sites. After being reduced to the iodide, the iodide can be desorbed quickly and transported away under the effect of high concentration grades generated by highly ordered mesopores. In comparison with three kinds of mesoporous carbons, the decline of mesopore ordering resulted in the reduction of current density and the negative shift of redox potential, indicating the reduced catalytic activity. For the carbon black CE, the reduction peaks are broad, displaying a slow I^-/I_3^- redox reaction owning to its unfavorable ions transport and large charge-transfer resistance (R_{ct}). In short, EIS, Tafel-polarization, and CV measurements are good ways to better understand the influence of mesopore ordering on the electrocatalytic activities of mesoporous carbon CEs.

4. CONCLUSIONS

Three kinds of mesoporous carbons were prepared by the facile organic-organic self-assembly method with different molar ratios of formaldehyde to resorcinol under the catalysis of critic acid. The prepared mesoporous carbons with different mesopore ordering were used as counter electrodes for DSSCs. The photovoltaic performance of the DSSCs assembled with mesoporous carbon CEs is correlated with the mesopore ordering. Especially, the electrocatalytic activity of highly ordered mesoporous carbon MC-2 CE is greatly enhanced in comparison with ordered mesoporous carbon MC-1 and disordered mesoporous carbon MC-3 CEs, due to superior ions transportation capacity based on its highly ordered mesopore channels and good electrocatalytic activity from abundant active sites. Besides, a mass production of highly ordered mesoporous carbons from citric acid catalytically synthesized phenolic resin would supply a green and low-cost counter electrode material for the DSSC, which can accelerate the progress of its commercialization in the future.

ACKNOWLEDGMENT

This work was supported by the National Natural Science Foundation of China (21076056 and 21073099), the Specialized Research Fund for the Doctoral Program of Higher Education (20110031110016), the Program for Innovative Research Team in University (IRT1059, IRT13022), the 111 project (B12015), and the Key Laboratory of Advanced Catalytic Materials in Zhejiang Normal University (ZJHX201301).

REFERENCES

[1] B. O'Regan, M. Grätzel, Nature 353 (1991) 737-740.

[2] Y. Chiba, A. Islam, Y. Watanabe, R. Komiya, N. Koide, L. Han, Jpn.J.Appl.Phys. 45 (2006) L638-L640.

[3] S. Zhang, X. Yang, Y. Numata, L. Han, Energy Environ. Sci. 6 (2013) 1443-1464.

[4] T.Y. Ma, Y.S. Wei, T.Z. Ren, L. Liu, Q. Guo, Z.Y. Yuan, ACS Appl. Mater. Interfaces 2 (2010) 3563-3571.

[5] T.-L. Hsieh, H.-W. Chen, C.-W. Kung, C.-C. Wang, R. Vittal, K.-C. Ho, J. Mater. Chem. 22 (2012) 5550-5559.

[6] X. Yang, M. Yanagida, L. Han, Energy Environ. Sci. 6 (2013) 54-66.

[7] E. Olsen, G. Hagen, S. E. Lindquist, Solar Energy Mater. Solar Cells 63 (2000) 267-273.

[8] Y.-S. Wei, Q.-Q. Jin, T.-Z. Ren, Solid-State Electronics 63 (2011) 76-82.

[9] J.-M. Kim, S.-W. Rhee, Electrochim. Acta 83 (2012) 264-270.

[10] W. Kwon, J.-M. Kim, S.-W. Rhee, Electrochim. Acta 68 (2012) 110-113.

[11] K. Imoto, K. Takahashi, T. Yamaguchi, T. Komura, J.-i. Nakamura, K. Murata, Solar Energy Mater. Solar Cells 79 (2003) 459-469.

[12] J. Chen, K. Li, Y. Luo, X. Guo, D. Li, M. Deng, S. Huang, Q. Meng, Carbon 47 (2009) 2704-2708.

[13] J.G. Nam, Y.J. Park, B.S. Kim, J.S. Lee, Scripta Mater. 62 (2010) 148-150.

[14] H. Anwar, A.E. George, I.G. Hill, Solar Energy 88 (2013) 129-136.

[15] W.J. Lee, E. Ramasamy, D.Y. Lee, J.S. Song, ACS Appl. Mater. Interfaces 1 (2009) 1145-1149.

[16] S.-Q. Fan, B. Fang, J. H. Kim, B. Jeong, C. Kim, J.-S. Yu, J. Ko, Langmuir 26 (2010) 13644–13649.

[17] G. wang, L. Wang, W. Xing, S. Zhuo, Mater. Chem. Phys. 123 (2010) 690-694.

[18] S.Y. Jang, Y.G. Kim, D.Y. Kim, H.G. Kim, S.M. Jo, ACS Appl. Mater. Interfaces 4 (2012) 3500-3507.

[19] X. Wang, L. Zhi, K. Mullen, Nano Lett. 8 (2008) 323-327.

[20] J. D. Roy-Mayhew, D. J. Bozym, C. Punckt, I. A. Aksay, ACS Nano 4 (2010) 6203–6211.

[21] D. Sebastián, V. Baglio, M. Girolamo, R. Moliner, M.J. Lázaro, A.S. Aricò, J. Power Sources 250 (2014) 242-249.

[22] T. Peng, W. Sun, X. Sun, N. Huang, Y. Liu, C. Bu, S. Guo, X.-Z. Zhao, Nanoscale 5 (2013) 337-341.

[23] B. Zhao, H. Huang, P. Jiang, H. Zhao, X. Huang, P. Shen, D. Wu, R. Fu, S. Tan, J. Phys. Chem. C 115 (2011) 22615-22621.

[24] J. Xu, A. Wang, T. Zhang, Carbon 50 (2012) 1807-1816.

[25] L. Liu, F.-Y. Wang, G.-S. Shao, T.-Y. Ma, Z.-Y. Yuan, Carbon 48 (2010) 2644-2673.

[26] Y. Yan, F. Zhang, Y. Meng, B. Tu, D. Zhao, Chem. Commun. (2007) 2867-2869.

[27] C. Liang, S. Dai, J. Am. Chem. Soc. 128 (2006) 5316-5317.

[28] L. Liu, F.-Y. Wang, G.-S. Shao, Z.-Y. Yuan, Carbon 48 (2010) 2089-2099.

[29] F. Zhang, Y. Meng, D. Gu, Y. Yan, C. Yu, B. Tu, D. Zhao, J. Am. Chem. Soc. 127 (2005) 13508-13509.

[30]L. Liu, Q.-F. Deng, T.-Y. Ma, X.-Z. Lin, X.-X. Hou, Y.-P. Liu, Z.-Y. Yuan, J. Mater. Chem. 21 (2011) 16001-16009.

[31] G.-P. Hao, W.-C. Li, S. Wang, G.-H. Wang, L. Qi, A.-H. Lu, Carbon 49 (2011) 3762-3772.

[32] A.-H. Lu, B. Spliethoff, F. Schüth, Chem. Mater. 20 (2008) 5314–5319.

[33] X. Wang, C. Liang, S. Dai, Langmuir 24 (2008) 7500-7505.

[34] X. Zhao, A. Wang, J. Yan, G. Sun, L. Sun, T. Zhang, Chem. Mater. 22 (2010) 5463-5473.

[35] Y. Huang, H. Cai, D. Feng, D. Gu, Y. Deng, B. Tu, H. Wang, P.A. Webley, D. Zhao, Chem. Commun. (2008) 2641-2643.

[36] D. Liu, J.-H. Lei, L.-P. Guo, D. Qu, Y. Li, B.-L. Su, Carbon 50 (2012) 476-487.

[37] D. Wu, Z. Li, Y. Liang, X. Yang, X. Zeng, R. Fu, Carbon 47 (2009) 916-918.

[38] N.P. Wickramaratne, V.S. Perera, B.-W. Park, M. Gao, G.W. McGimpsey, S.D. Huang, M. Jaroniec, Chem. Mater. 25 (2013) 2803-2811.

[39] Y. Liu, Q. Liu, J. Gu, D. Kang, F. Zhou, W. Zhang, Y. Wu, D. Zhang, Carbon 64 (2013) 132-140.

[40] S. Zhang, L. Chen, S. Zhou, D. Zhao, L. Wu, Chem. Mater. 22 (2010) 3433-3440.

[41] A. Sadezky, H. Muckenhuber, H. Grothe, R. Niessner, U. Pöschl, Carbon 43 (2005) 1731-1742.

[42] X. Zhang, J. Zhang, Y. Cui, J. Feng, Y. Zhu, J. Appl. Polym. Sci. 128 (2013) 75-79.

[43] B. Fang, S.-Q. Fan, J. H. Kim, M.-S. Kim, M. Kim, N. K. Chaudhari, J. Ko, J.-S. Yu, Langmuir 26 (2010) 11238–11243.

[44] F. Gong, H. Wang, X. Xu, G. Zhou, Z.S. Wang, J. Am. Chem. Soc. 134 (2012) 10953-10958.

[45] M. Wang, A. M. Anghel, B. Marsan, N. C. Ha, N. Pootrakulchote, S. M. Zakeeruddin, M. Grätzel, J. Am. Chem. Soc. 131 (2009) 15976–15977.

[46] M. Wu, X. Lin, A. Hagfeldt, T. Ma, Angew. Chem. Int. Ed. 50 (2011) 3520-3524.

[47] G.R. Li, F. Wang, J. Song, F.Y. Xiong, X.P. Gao, Electrochim. Acta 65 (2012) 216-220.

[48] M. Wu, Y. Wang, X. Lin, N. Yu, L. Wang, L. Wang, A. Hagfeldt, T. Ma, Phys. Chem. Chem. Phys. 13 (2011) 19298-19301.

[49] J. Halme, M. Toivola, A. Tolvanen, P. Lund, Solar Energy Mater. Solar Cells 90 (2006) 872-886.

[50] Y. Gao, L. Chu, M. Wu, L. Wang, W. Guo, T. Ma, J. Photochem. Photobio. A 245 (2012) 66-71.

[51] Z. Li, F. Gong, G. Zhou, Z.-S. Wang, J. Phys. Chem. C 117 (2013) 6561-6566.

[52] G. Yue, J. Wu, Y. Xiao, M. Huang, J. Lin, J.-Y. Lin, J. Mater. Chem. A 1 (2013) 1495-1501.

[53] M. J. Ju, J. C. Kim, H. J. Choi, I. T. Choi, S. G. Kim, K. Lim, J. Ko, J. J. Lee, I. Y. Jeon, J. B. Baek, H. K. Kim, ACS Nano 7 (2013) 5243-5250.

[54] M. Wu, X. Lin, A. Hagfeldt, T. Ma, Chem. Commun. 47 (2011) 4535-4537.

[55] N. Papageorgiou, Coord. Chem. Rev. 248 (2004) 1421-1446.

[56] S.-H. Park, B.-K. Kim, W.-J. Lee, J. Power Sources 239 (2013) 122-127.

[57] Y. Liao, K. Pan, L. Wang, Q. Pan, W. Zhou, X. Miao, B. Jiang, C. Tian, G. Tian, G. Wang, H. Fu, ACS Appl. Mater. Interfaces 5 (2013) 3663-3670.

Research Highlights

- Ordered mesoporous carbons as counter electrode material for dye-sensitized solar cells
- The effect of structural mesopore ordering on the photovoltaic performance of DSSCs.
- High-performance cells with highly ordered mesoporous carbon counter electrode
- Excellent energy conversion efficiency of 6.06%, comparable to that of the cell with Pt counter electrode (6.29%)